A novel approach to simulate pollutant dispersion in the built environment

Building and Environment 170 (2020) 106604

Contents lists available at ScienceDirect

Building and Environment

journal homepage: http://www.elsevier.com/locate/buildenv

A novel approach to simulate pollutant dispersion in the built environment: Transport-based recurrence CFD

Yaxing Du [a], Bert Blocken [b,c], Stefan Pirker [a,*]

[a] Department of Particulate Flow Modelling, Johannes Kepler University, Linz, Austria
[b] Department of the Built Environment, Eindhoven University of Technology, Eindhoven, Netherlands
[c] Department of Civil Engineering, KU Leuven, Leuven, Belgium

ARTICLE INFO

Keywords:
Transport-based recurrence CFD (rCFD)
Large eddy simulation (LES)
Novel diffusion model
Pollutant dispersion
Urban environment

ABSTRACT

The large-scale practical application of Large-Eddy Simulation (LES) for predicting long-term wind flow and pollutant dispersion in urban areas is inhibited mainly by the associated very large computational costs. To overcome this difficulty, the present study, for the first time, applies transport-based recurrence Computational Fluid Dynamics (rCFD) to simulate atmospheric pollutant dispersion around a building. A novel diffusion model is proposed to accurately predict pollutant transport with rCFD. To illustrate the feasibility and advantages of rCFD, pollutant dispersion around an isolated cubical building with a rooftop vent, immersed in neutral atmospheric boundary layer flow is used as a case study and both LES and rCFD simulations are conducted. It is shown that rCFD simulation results agree well with those from LES both in terms of mean and fluctuating concentrations while the simulation wall-clock time drops from 222 h to 16 min. The application of four evaluation metrics (FAC2, FB, NMSE and R) indicates very good agreement between LES and rCFD results. Another major advantage of rCFD is that different pollutant events can be simulated promptly once the database has been stored for a given flow configuration, as shown by the comparison of LES and rCFD results for two other cases with different release locations. This study extends the application of transport-based rCFD to pollutant dispersion in the built environment and indicates that rCFD is a promising approach to facilitate the large-scale practical application of LES for this type of applications.

1. Introduction

Rapid urbanization entails outdoor air quality problems due to toxic and/or odorous exhausts such as vehicle exhaust and factory fumes [1]. Air pollution in the urban environment has become a pressing issue all over the world over the last decades [2,3]. Pollutant transport and dispersion is mainly determined by source location, meteorological conditions and the geometrical features of the urban environment. High pollutant concentrations in urban areas cannot only affect the outdoor air quality, but also influence the indoor air quality by air infiltration through windows and doors [4]. In the past, for practical applications, empirical or semi-empirical models such as the Gaussian dispersion model and the ASHRAE model [5] have been frequently used. These models are based on a statistical distribution of atmospheric dispersion and allow a fast estimate of urban air pollutant concentrations [6,7]. However, these models have limited applicability for near-field pollutant dispersion where the influence of individual building obstacles plays an important role [2,8,9]. Especially for near-field pollutant dispersion, it is very important to be able to provide more accurate simulations towards the provision of effective solutions for controlling and maintaining outdoor air quality.

Near-field pollutant dispersion around buildings and in the built environment has also been widely investigated by numerical simulation with Computational Fluid Dynamics (CFD) [10–12]. Because of the associated computational costs, most studies adopted the steady Reynolds-Averaged Navier-Stokes (RANS) approach rather than Large-Eddy Simulation (LES) [13–19]. However, steady RANS simulations can only provide mean wind flow and concentration fields and do not capture the inherently transient behaviour that is characteristic of wind flow around buildings. On the other hand, Large-Eddy Simulation (LES) is intrinsically superior in providing more accurate results for wind flow and pollutant dispersion in urban environments [20–23]. Tominaga and Stathopoulos [24] reported significant differences in the distribution of eddy diffusivity from LES and RANS. Gousseau et al. [20] performed both LES and RANS for pollutant dispersion around an

* Corresponding author.
E-mail addresses: yaxing.du@jku.at (Y. Du), B.J.E.Blocken@tue.nl (B. Blocken), stefan.pirker@jku.at (S. Pirker).

https://doi.org/10.1016/j.buildenv.2019.106604
Received 30 October 2019; Received in revised form 9 December 2019; Accepted 13 December 2019
Available online 18 December 2019

Nomenclature

Greek letters

$\varepsilon(z)$	turbulence dissipation rate, m^2/s^3
$\sigma_{P,LES}$	standard deviation of P_{LES}, -
$\sigma_{P,r}$	standard deviation of P_r, -
μ_{eff}	effective subgrid-scale viscosity, kg/m·s
τ_{DB}	monitoring period of recurrence statistics, s
τ_{ij}	effective stress tensor, N/m^2
Φ	field quantity, -

List of symbols

$\bar{c}$	spatially filtered concentration, kg/m^3
c	local concentration, kg/m^3
C_0	reference concentration, kg/m^3
c'_{rms}	root-mean-square of concentration fluctuation, kg/m^3
C_μ	constant, 0.09
D_{eff}	effective diffusivity, m^2/s
E	relative error, -
E_{avg}	average relative error, -
E_{max}	maximum relative error, -
f_{h-p}	highest peak frequency, Hz
f_{max}	maximum frequency, Hz
f_{min}	minimum frequency, Hz
H_b	building height, m
I_c	local fluctuation intensity, -
$k(z)$	turbulence kinetic energy, m^2/s^2
K_c	non-dimensional concentration coefficient, -
$K_{c,LES}$	K_c value from LES, -
$K_{c,WT}$	K_c value from wind tunnel test, -
L	computational domain length, m
N_{DB}	frame number of recurrence database, -
N_e	end frame, -
N_s	start frame, -
N_{seq}	number of consecutive frames, -
P_r	predicted results from rCFD, -
P_{LES}	predicted results from LES, -
Q_e	source mass flow rate, kg/s
r	spatial position, -
p	pressure, Pa
$\bar{s}$	local pollutant source term, kg/s
t_f	flow-through time, s
t^*	non-dimensional sampling time duration, -
Δt_{CFD}	time step of full CFD, s
Δt_{rec}	time step of rCFD, s
TI	turbulence intensity, -
u_i	velocity components, m/s
U	velocity magnitude, m/s
U_b	wind speed at building height, m/s
W_e	exhaust speed, m/s

isolated building and found counter-gradient turbulent diffusion in the streamwise direction by LES, while steady RANS with the standard gradient-diffusion hypothesis assumes the exact opposite. Ai and Mak [25] revealed the transient characteristics of inter-unit pollutant dispersion by LES, which helped unravel the associated dispersion mechanisms and guided control strategies for epidemic disease. Moonen et al. [26] demonstrated that the transient flow character has a considerable influence on the simulation accuracy of the predicted air exchange rate in a city block. However, Tominaga and Stathopoulos [10] noted that the computational time for LES is usually 10–25 times higher than for RANS, which restricts the application of LES mostly to isolated building scenarios or to research studies rather than practical engineering consultancy work. This indicates the need for an innovative method to reduce the computational cost for LES for pollutant dispersion in urban environments without compromising the accuracy and reliability of the simulations.

In the present paper, for the first time, transport-based rCFD is applied to simulate atmospheric pollutant dispersion around a building. This approach is adopted because of its remarkable computational efficiency [27]. Beyond a pure application of an existing method, in this paper, transport-based rCFD is significantly further developed to accurately reproduce the pollutant dispersion. The existing (rudimentary) global one-step diffusion concept is thoroughly revised and further developed here, since the turbulent diffusivity plays a crucial role in the atmospheric dispersion process [10]. In terms of application, this paper focuses on the pollutant dispersion around an isolated cubical building with a rooftop vent immersed in a neutrally-stratified atmospheric boundary layer. This configuration was first studied experimentally by Li and Meroney [28] and it thereafter served as validation benchmark for several numerical studies (e.g. Refs. [16,20,29–32]).

The paper is structured as follows: in Section 2, the existing transport-based rCFD approach is presented together with the novel subgrid-scale diffusion model. In Section 3, conventional LES of the cubical building case is conducted and compared to wind tunnel test data to establish a reliable validation basis for the rCFD simulations thereafter. In Section 4, the predictive capability of transport-based rCFD is evaluated by means of a set of evaluation metrics applied to vertical profiles of time-averaged and fluctuating concentrations downstream of the building. Finally, Section 5 discusses the existing limitations, prediction accuracy and computational cost of this novel modelling framework.

2. Recurrence CFD approach

2.1. Introduction to recurrence CFD

There is a natural quest for novel approaches that enable accurate scale resolved simulations with considerably reduced computational costs. Proper Orthogonal Decomposition (POD) methods have emerged over the years, which first transform a pseudo-periodic flow into characteristic modes and then use these modes to efficiently time-extrapolate this flow. A review on POD methods can be found in Ref. [33]. More recently, POD has been combined with parallel time-stepping, which reportedly results in an overall speed-up of two orders of magnitude [34].

In the present paper, we adopt an alternative approach labelled recurrence CFD (rCFD), which was developed in the field of chemical engineering [27,35–37]. Conceptually, rCFD employs a similar two-phase strategy as POD techniques (see Fig. 1): in the first phase of data-generation, conventional (expensive) CFD simulations are used to generate a characteristic database for the pseudo-periodic flow under consideration; and in the second phase of data-exploitation, this database is used to simulate transport processes of passive scalars, such as the dispersion of species, based on a recurrence process of sequence stitching.

In the first version of rCFD, the characteristic database was established by a series of snap-shots of Eulerian velocity fields [35,36]. Based on a recurrence analysis of those snap-shots, a Markov-alike recurrence process consequently constructs an artificial flow candidate, which can proceed beyond the restricted time-span covered by the database [35,36]. Finally, passive scalars can be traced by solving conventional transport equations. Similar to recent POD approaches, this flow-based

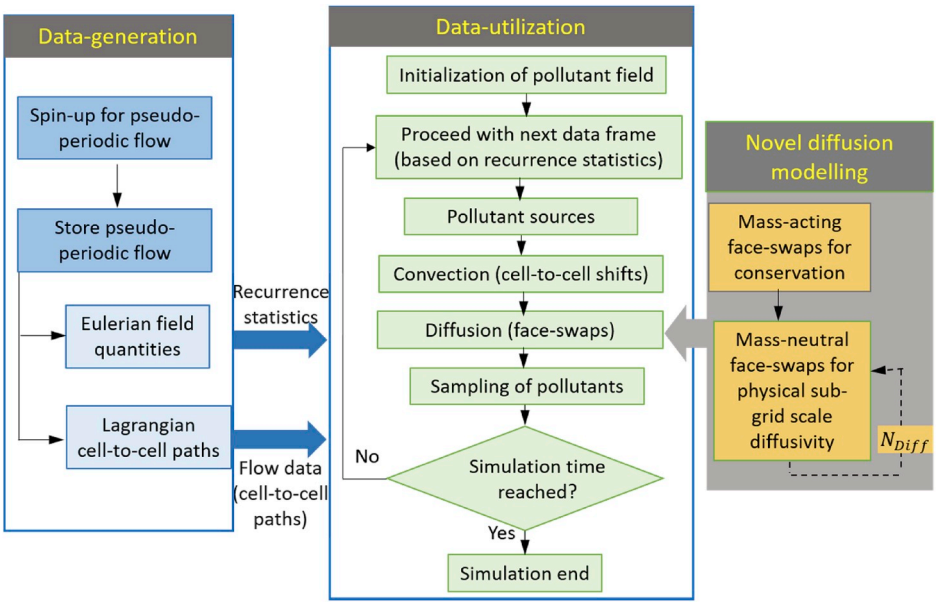

Fig. 1. Flow sheets of the rCFD simulation approach.

rCFD speeds up conventional LES based CFD simulations by more than two orders of magnitude [35,36].

In the second version of rCFD, a Lagrangian representation of fluid flow is used instead of the Eulerian field representation [27,37]. In this case, the fluid flow is characterised by the movement of massless tracer particles. Consequently, the database is not filled by snap-shots of (Eulerian) field quantities but by snap-shots of (Lagrangian) tracer movements. In discretised form, the latter transforms to snap-shots of convective cell-to-cell paths [27]. Applying the same Markov-alike recurrence process, once again a flow candidate can be extrapolated beyond the time-span of the database – this time by applying transport (i.e. cell-to-cell shift) operations rather than by reconstructing the flow field itself. On top of this Lagrangian flow representation, passive scalars pass their information along the pre-set paths of the cell-to-cell connections. In a sense, this transport-based version of rCFD circumvents the construction of artificial flow fields and directly shortcuts to a discretised representation of physical convection.

In terms of computational time, the transport-based rCFD outperforms the flow-based rCFD by another two orders of magnitude, so in total, transport-based rCFD is about four orders of magnitude faster than conventional full LES based on CFD simulation time [27,37]. This tremendous speed-up can be explained by the fact that in transport-based rCFD neither the flow equations (like in conventional CFD) nor the scalar transport equations (like in flow-based rCFD) are solved. Instead, transport-based rCFD represents a fully data-based method, with the passive scalars being propagated along their pre-defined cell-to-cell paths. Detailed algorithmic flow-sheets of this method are given in Refs. [27,37].

2.2. Existing recurrence CFD approach

For the sake of readability, first the basic ingredients of transport-based rCFD (hereafter, rCFD) are stated and afterwards the novel diffusion model is presented. Basically, the rCFD approach can be divided into two parts: data-generation and data-utilization. The data-generation is achieved by CFD simulation with LES and the data-utilization is based on Eulerian field quantities, recurrence statistics and Lagrangian cell-to-cell connectivity patterns. The flow sheets of the rCFD approach are presented in Fig. 1. The detailed methodology of rCFD is presented below and can also be found in the previous publications in the realm of chemical engineering [27,35–37].

To obtain a suitable database for rCFD simulation, a proper recording time step (Δt_{rec}) has to be specified for the representation of the pseudo-periodic flow under consideration. This recording time step can be deduced from a spectral analysis of the unsteady fluxes at sample points by relating it to the highest peak frequency (f_{h-p}) of the spectrum,

$$\Delta t_{rec} < 1/f_{h-p} \tag{1}$$

Alternatively, a proper recording time step can be calculated by analysing the time evolution of a given field quantity Φ by:

$$\Delta t_{rec} \equiv \frac{1}{f_{max}} \ll \sqrt{\langle \Phi^2 \rangle / \langle \dot{\Phi}^2 \rangle}, \tag{2}$$

where $\langle \cdot \rangle$ indicates time averaging, $\dot{\Phi}$ is the time derivative of Φ and f_{max} represents the maximum flow frequency, which can be resolved by this recording time step. While these two estimates provide a physically motivated upper limit for the recording time step, it should be balanced with the quest for computational efficiency, such that still

$$\Delta t_{rec} \gg \Delta t_{CFD}, \tag{3}$$

with Δt_{CFD} being the time step of the full CFD simulations.

Once the recording time step has been determined, a database of N_{DB} consecutive frames of Eulerian field quantities together with corresponding Lagrangian cell-to-cell paths can be recorded. Note that in transport-based rCFD, the Eulerian field quantities are stored just for the purpose of evaluating recurrence statistics (described further below) while the Lagrangian cell-to-cell paths are utilised for the later pollutant dispersion modelling. The total time-span covered by the database, $\tau_{DB} = N_{DB}\ \Delta t_{rec}$, further defines a minimum flow frequency $f_{min} = 1/\tau_{DB}$, which can be represented by this database. Concluding, any subsequent rCFD simulations can only resolve flow dynamics in-between these limiting frequencies of $f_{min} = 1/\tau_{DB}$ and $f_{max} = 1/\Delta t_{rec}$.

In a next step, the similarity for pairs of frames of Eulerian field quantities at two instances of time t and t' are evaluated by a global recurrence norm (*rNorm*):

$$rNorm(t,t') = \frac{\int d^3r \left(\Phi(\boldsymbol{r},t) - \Phi(\boldsymbol{r},t')\right)^2}{max_{t,t'} \int d^3r \left(\Phi(\boldsymbol{r},t) - \Phi(\boldsymbol{r},t')\right)^2} \tag{4}$$

Ideally, Φ should represent the physical core phenomenon of the flow of interest, and r is spatial position in Cartesian coordinate. In this

study, the dynamic behaviour of the vertical shear layers around the cubical building have been identified as flow-specific core phenomenon. Consequently, the vertical vorticity of the velocity field has been chosen as field quantity Φ. In order to further focus on this core phenomenon, small contributions, $\Phi < \Phi_{small}$, are excluded from the evaluation of $rNorm(t,\acute{t})$ in order to reduce data noise.

All together, these pairwise evaluations of $rNorm(t,\acute{t})$ span a symmetric recurrence matrix (*rMatrix*) with zero diagonal (an example will be given in Fig. 6c). A local off-diagonal minimum indicates that the corresponding frame pairing can be considered as similar with respect to the chosen norm (and vice versa; an off-diagonal maximum indicates that these frames represent dominantly different states).

The *rMatrix* serves as base for the recurrence process triggering a kind of sequence stitching procedure (illustrated in Fig. 2). Starting from a start-frame N_s, a sequence of N_{seq} consecutive frames (with N_{seq}, for every new sequence, randomly chosen in between $1 < N_{seq} < N_{DB}$) is replayed from the database (arrow 1 in the figure). After this initial sequence, the start-frame of the next sequence is chosen by looking for a local off-diagonal minimum of the pairwise recurrence norm between the old end-frame (N_e in the figure) and the new start-frame. Next, the second random-length sequence (arrow 2 in the figure) is chosen and is replayed, before the start-frame of the third sequence is chosen analogously and so forth. Note that the position of the new start-frame in the database can be in front of or behind the old end-frame. In the latter case, the third sequence is based on data which have been recorded before that of the second frame in Fig. 2.

In transport-based rCFD, pollution dispersion is finally addressed by cell-to-cell shift and face swap operations. First, at the start of a recurrence time-step Δt_{rec}, local sources (e.g. the rooftop vent of the cubical building here) are considered by changing the field values accordingly. Second, the convection of the pollutant is mimicked by shifting this concentration field along the cell-to-cell paths as defined in the current frame of the database. Third, the diffusion of the pollutant is accounted for by local face-swaps, which implies that high concentration cells shift part of their species towards neighbouring cells with a lower concentration. After this, the next frame in the database will be chosen according to the recurrence process described above (detailed algorithmic flow-sheets of these operations can be found in Ref. [27]).

2.3. Novel subgrid-scale diffusion model

The rudimentary representation of physical turbulent diffusion by face-swap operations (explicit one-step diffusion) can be seen as major weak point of transport-based rCFD [27]. This is further aggravated by the fact that these face-swap operations are not only used to model physical subgrid-scale diffusion but additionally used to control global mass/species balances. For the latter, a small mass defect is introduced into those swap operations, which on a global level controls mass/species conservation. While this rough one-step modelling of physical subgrid-scale diffusion and mass/species conservation has been proven to be sufficient for specific applications in chemical engineering [27], it certainly has to be improved for the case of atmospheric pollutant dispersion.

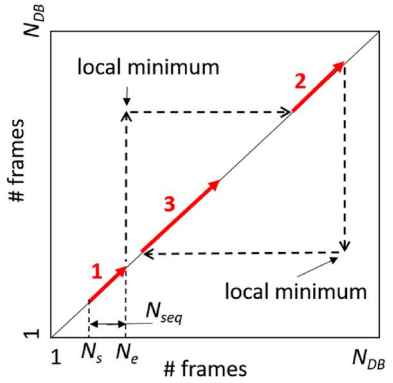

Fig. 2. Sketch for the construction of recurrence path.

First and foremost, the physical subgrid-scale diffusion modelling is added as part of the novel diffusion modelling and it is separated from the mass conservation control. The one-step face-swap operation with mass-defects is still used for conservation control. However, these mass-defects are adapted dynamically to minimise the artificial diffusive impact of those face swaps. Second, the amount of physical subgrid-scale diffusion is linked to the local turbulent diffusivity. In the framework of standard Smagorinsky LES, the turbulent subgrid-scale diffusive face flux is related to the sub-grid turbulent viscosity (by the sub-grid turbulent Schmidt number) [38,39]. Consequently, local sub-grid viscosities have to be provided by the recurrence database in addition to the information about Lagrangian cell-to-cell paths. Once local values for sub-grid viscosity are available, the turbulent subgrid-scale diffusive face flux can be estimated. Because these turbulent subgrid-scale fluxes are too large for just one face-swap operation (such large flux values would inevitably lead to numerical instabilities), several face-swaps with lower turbulent subgrid-scale flux values will be made during the rCFD simulation in order to finally obtain the required amount of turbulent subgrid-scale diffusion.

To sum up, the face-swap operations are separated into mass/species conservation and the modelling of physical turbulent diffusion. While the first is realised by just one mass-acting face-swap operation (as least invasive as possible), the latter is addressed by repeating face-swaps until turbulent physical subgrid-scale diffusion is achieved.

2.4. Numerical implementation

Since transport-based rCFD runs on the same grid as full CFD, the establishment of the recurrence database is straightforward: Eulerian cell values and Lagrangian cell-to-cell paths are stored during conventional LES modelling. The rCFD functionalities are realised within the framework of ANSYS Fluent V19.2 via User Defined Functions (UDFs) [38]. After storing the database, solver functionality is not used except for grid access functions (e.g. cell to face pointers), parallel communication (by MPI-macros) and post-processing. Note that rCFD has also been applied in other software like OpenFOAM and LIGGGHTS [40].

3. Conventional CFD simulation

3.1. Large eddy simulation (LES)

The LES approach is employed for two reasons: the establishment of the recurrence database for the pseudo-periodic flow field and (later on) the validation of rCFD predictions of pollutant dispersion.

Under the assumption of isothermal and incompressible flow, the governing flow equations for LES read

$$\frac{\partial \overline{u}_i}{\partial x_i} = 0 \tag{5}$$

$$\frac{\partial(\rho\overline{u}_i)}{\partial t} + \frac{\partial\left(\rho\overline{u_i u_j}\right)}{\partial x_j} = \frac{\partial \overline{p}}{\partial x_i} - \frac{\partial \tau_{ij}}{\partial x_j} \tag{6}$$

Here, u_i and p are the Cartesian velocity components and the pressure with the overbars denoting spatial filtering and τ_{ij} is the effective stress tensor summarizing molecular and turbulent momentum diffusion. In the standard Smagorinsky model, the unresolved sub-grid diffusion is addressed by the sub-grid viscosity [39].

The governing equation for the pollutant concentration field can be written as

$$\frac{\partial \overline{c}}{\partial t}+\frac{\partial\left(\overline{cu_j}\right)}{\partial x_j}=-\frac{\partial}{\partial x_j}D_{eff}\frac{\partial \overline{c}}{\partial x_j}+\overline{s}, \tag{7}$$

where, $\overline{c}$ is the spatially filtered pollutant concentration and $D_{eff}=\mu_{eff}/Sc_t$ is the effective diffusivity. Finally, $\overline{s}$ indicates local pollutant source.

3.2. Case description

The benchmark wind tunnel test case conducted by Li and Meroney [28] is adopted. In the present study, only the approaching wind direction of 0° is considered, which is perpendicular to the building's windward facade. The cubical building with a height H_b of 0.05 m was immersed in a neutrally stratified turbulent atmospheric boundary layer. The incident mean wind speed profile followed a power law with exponent 0.19. The mean wind speed at building height U_b was 3.3 m/s. The longitudinal turbulence intensity was 11.8% at building height. The Reynolds number based on building height was 1.1×10^4. The pollutant was a mixture of helium with air that was assumed to act as a passive pollutant. It was continuously released from a central rooftop vent. The momentum ratio, defined as the ratio of the exhaust speed to the reference wind speed at building height (W_e/U_b), was 0.19. Measurements of the pollutant concentration were made on the roof surface, the leeward façade surface and in the building wake. More detailed information on the experiment can be found in Ref. [28]. In the remainder of the present paper, the non-dimensional concentration coefficient (K_c) is used to describe the concentration distribution:

$$K_c=c/C_0 \tag{8}$$

where, c is the local concentration and C_0 is the reference concentration at the source location.

$$C_0=\frac{Q_e}{H_b^2U_b} \tag{9}$$

where, $Q_e$is the time-averaged mass flow rate at the source location.

For the concentration fluctuations, the local fluctuation intensity (I_c) [41] is used here, which is defined as the ratio between the root-mean-square value of the concentration fluctuation to the mean concentration at the same location:

$$I_c=c'_{rms}/c \tag{10}$$

The CFD simulations are performed at wind tunnel scale. The LES simulation is initialized from a preliminary converged steady Reynolds-averaged Navier-Stokes (RANS) simulation with the Re-Normalisation Group (RNG) k-ε turbulence model [38]. The standard Smagorinsky-Lilly model [39] with constant $C_s = 0.1$, is applied for subgrid-scale modelling. For the near-wall treatment, the LES default wall function is used [38]. The computational domain is depicted in Fig. 3 together with the boundary conditions. The domain size is chosen based on the best practice guidelines [42–44]. The domain is discretised with 1.2 million hexahedral cells using the surface-grid extrusion method [45]. The best practice guidelines are applied in the grid generation [42,44,46]. In addition, the distance y_P of the wall-adjacent cell centrepoint to the building surfaces is 0.00125 m, which results in a y* value in the range of 0–4 (mostly around 1). The stretching factor was kept below 1.08. Detailed information on the grid sensitivity study is presented in Section 3.3. The vertical inlet profiles of the mean wind speed and longitudinal turbulent intensity are obtained directly from the wind tunnel test. The turbulence kinetic energy (k(z)) and the dissipation rate (ε(z)) are calculated by Equations (11) and (12) [38]. The vortex method [47] with 190 vortices is used to generate the turbulent inflow. Second-order schemes are adopted for the temporal and spatial derivatives, and SIMPLEC is used for pressure-velocity coupling. For both full CFD and rCFD, the data sampling starts when the wind velocity shows pseudo-periodic features, which is after two flow-through times ($t_f = L/U_b$, where L is the length of the computational domain). The time averaged values are obtained for a sampling duration of non-dimensional time $t^*\left(t^*=\frac{t\times U_b}{H_b}\right)=1320$, where t is the simulation flow time. This corresponds to 40 flow-through times. These numerical settings will be used in the remainder of the paper for both full LES and rCFD simulation.

$$k(z)=1.5(TI(z)\times U)^2 \tag{11}$$

$$\varepsilon(z)=C_\mu^{0.5}k(z)\frac{dU}{dz} \tag{12}$$

where, $TI(z)$ is turbulence intensity measured in the wind tunnel test, and U is velocity magnitude. C_μ is a constant equal to 0.09.

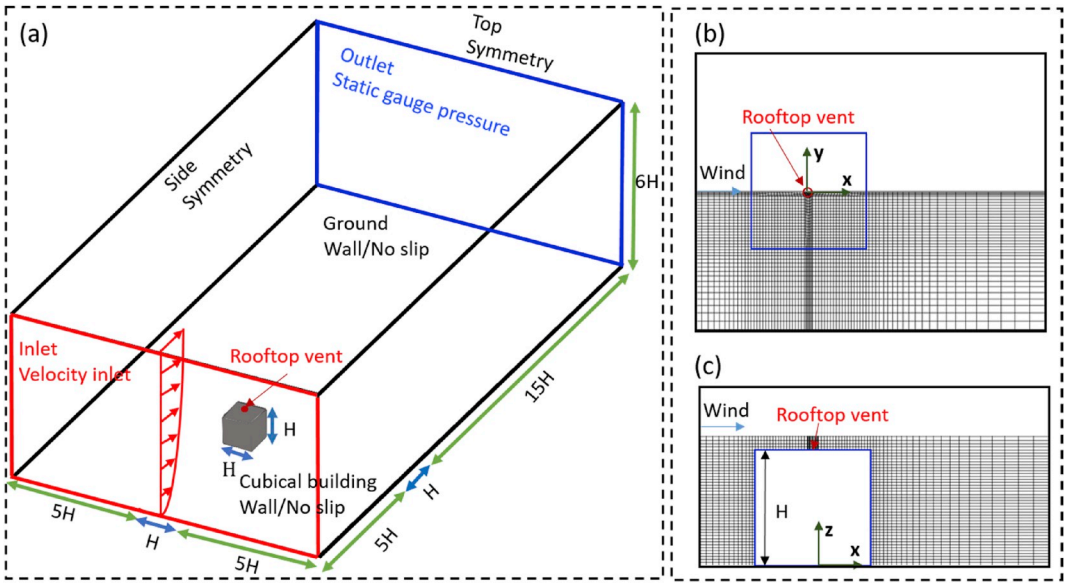

Fig. 3. (a) Computational domain and boundary conditions; (b,c) computational grid with total cell count of 1.2 million (medium grid): (b) in horizontal plane at building height and (c) in vertical centre-plane.

3.3. Verification of full CFD

In terms of the spatial resolution, three grids are constructed, a coarse, medium and fine grid, with total cell counts of 0.7 million, 1.2 million and 2.6 million, respectively. Away from the cubical building, the stretching rate is kept below 1.08 to limit truncation and commutation errors [44]. For the temporal resolution, three fixed time steps are tested: $\Delta t^* = 0.020$, 0.033, and 0.066 ($\Delta t^* = \Delta t_{CFD} \times U_b / H_b$, Δt_{CFD} is the actual time step in the CFD simulation). The CFL numbers (=uΔt/ d, where u is local velocity and d is local cell size) of $\Delta t^* = 0.033$ and 0.020 for the medium grid are both below one. The results are presented along three vertical lines in the vertical centre-plane downstream of the building in Fig. 4. The grid sensitivity analysis is conducted with time step of $\Delta t^* = 0.033$, and the time-step sensitivity analysis is conducted with the medium grid. A subtle change can be observed from the medium grid to fine grid for the three vertical lines in Fig. 4a–c, whereas the change from the coarse grid to medium grid is large. The average values of the deviations between the medium grid and the fine grid are 3%, 4% and 8% for the three vertical lines, respectively. The average values of the deviations between the coarse grid and the medium grid are 32%, 46% and 48% for the same three vertical lines. Similarly, as can be seen from Fig. 4d–f, the results of time step $\Delta t^* = 0.033$ show slight differences from that of $\Delta t^* = 0.020$ for the three vertical lines, while the differences between the results from $\Delta t^* = 0.066$ and other two time steps are large. The average values of the deviations between $\Delta t^* = 0.020$ and $\Delta t^* = 0.033$ are 7%, 9% and 9% for the three vertical lines, whereas those between $\Delta t^* = 0.033$ and $\Delta t^* = 0.066$ are 59%, 58% and 46%. Thus, the medium grid and the time step $\Delta t^* = 0.033$ are retained for the full LES cases; and the medium grid resolution is also used for the following rCFD cases.

3.4. Validation of conventional CFD

The values of the time-averaged concentration coefficient (K_c) and the local fluctuation intensity (I_c) obtained from LES on the medium grid and with $\Delta t^* = 0.033$ are compared with the wind tunnel test data by Li and Meroney [28,41] in Fig. 5. It is clear that a good agreement has been achieved between the LES results and wind tunnel data in terms of time-averaged concentration (Fig. 5a–c) and concentration fluctuation (Fig. 5d–f) The relative error E (%) is defined as:

$$E = 100\% \times \frac{|K_{c,WT} - K_{c,LES}|}{K_{c,WT}} \tag{13}$$

where $K_{c,WT}$ and $K_{c,LES}$ are the wind tunnel and LES computed K_c values, respectively. The average (E_{avg}) and maximum (E_{max}) values of the relative error are given in Fig. 5. For the time-averaged concentration comparison (Fig. 5a–c), the values of E_{avg} for the three vertical lines are around 10%, and all below 13%. Even though the value of E_{max} exceeds 20% for x/H = 1, the results are still acceptable. This deviation occurs at 1.5 times the building height where $K_{c,WT}$ value is relatively small. For the concentration fluctuation comparison (Fig. 5d–f), the values of E_{avg} for the three vertical lines are around 10%, and all below 12%.

4. Recurrence CFD simulations

4.1. Numerical settings

To investigate the transient nature of the velocity field and the pollutant concentration field, the instantaneous velocity and the instantaneous K_c of the pollutant are monitored at three points near the cubical building (Fig. 6a) during the LES modelling. P1 and P3 are located in the vertical central plane (y/H = 0) while P2 is located in the

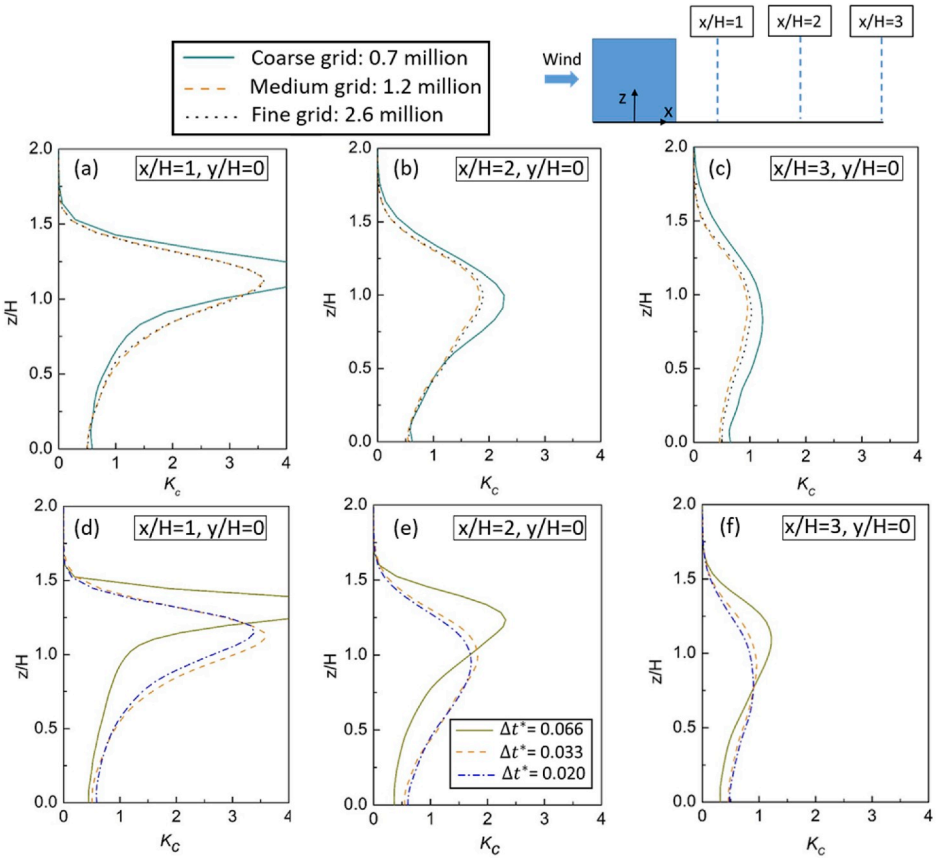

Fig. 4. Sensitivity analysis results: (a–c) grid sensitivity and (d–f) time-step sensitivity.

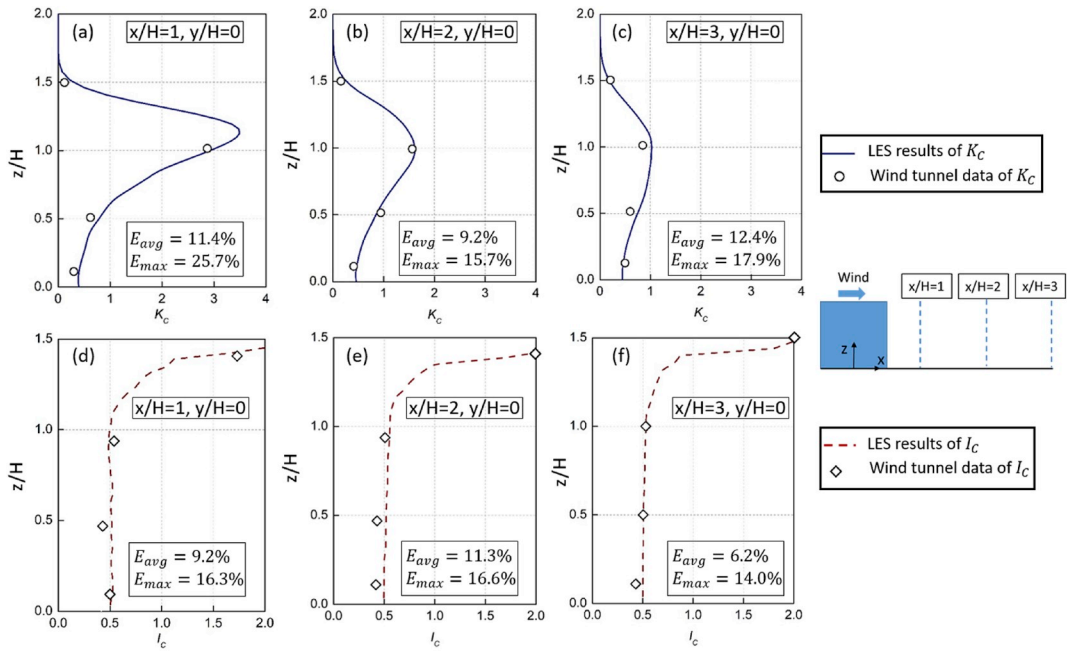

Fig. 5. Validation of full LES simulation by comparison with wind tunnel data.

plane y/H = 0.2. The spectral analysis of the fluctuating K_c values is presented in Fig. 6b, in which the pseudo-periodicity can be revealed by the absolute value of the Fourier-amplitude. According to Equation (2), the sampling frequency f_{max}, i.e. the frequency corresponding to the lowest Fourier amplitude, should be exceeded in order to ensure accurate interpolation for the storage data set ($\Delta t_{rec} = 1/f_{max}$). Thus, the Δt_{rec} for the rCFD simulation is set as 0.01 s since $f_{\max}$ is 100. Furthermore, 80 frames are recorded to construct the recurrence matrix (rMatrix, see Fig. 6c) which exhibits a nearly horizontal off-diagonal recurrence plateau, thus indicating that the pseudo-periodic nature of the flow is covered by the database [27]. In addition, Fig. 6c illustrates an example of the recurrence path reconstruction: starting from frame 10 (N_s in Fig. 2), seven consecutive frames are replayed (red arrow in the figure); and then the local off-diagonal minimum value of *rNorm* is found based on the rMatrix (here frame 60).

4.2. Results of mean concentration coefficient

Fig. 7 shows contours of the mean K_C for full LES and rCFD in the vertical centre-plane and in a horizontal plane at z/H = 1 (roof height) together with the iso-surfaces of mean $K_c = 0.5$ and 1 and the wall-clock time consumption (CPU time). Note that the time consumed for the spin-up process, before the flow shows pseudo-periodic characteristics in the computational domain, is the same for full LES and rCFD. The rCFD simulation with two different diffusion methods (e.g., one diffusion factor (global diffusion) and diffusivity related to local sub-grid eddy viscosity (novel diffusion model described in Section 2.3, local diffusion)) are also compared to illustrate the necessity of applying the novel diffusion model for pollutant dispersion as explained in Section 2.3. The contours in Fig. 7a–d shows that the rCFD results are similar to those by full LES, except that the rCFD simulation contours are less smooth due to the limited storage database. However, the downstream length and the shape of the concentration plumes by full LES and rCFD are very similar in the two planes. In the horizontal plane, the pollutant concentration in the separation bubble on the lateral sides of the building is reproduced by rCFD thanks to the novel diffusion model (see Fig. 7d versus 7f). The application of the novel diffusion model improves the prediction accuracy of rCFD and is thus used for the rest of the rCFD simulations in this paper. Overall, the prediction result from rCFD with the novel diffusion model agrees well with full LES with regard to the mean concentration contours. Note that after the spin-up process, the wall-clock time for full LES is 222 h while the wall-clock time for rCFD is only 16 min, which implies a 99.8% computational time reduction.

The time-averaged concentration plumes by full LES and rCFD for $K_C = 0.5$ and 1 are presented in Fig. 7h–k. It can be observed that the rCFD shapes of the time-averaged concentration plume are less smooth compared to LES. This artificial irregularity can be directly attributed to the discretization of the convective fluxes by means of cell-to-cell shifts. There are also subtle differences between the isosurfaces in terms of length and shape in the downstream regions, which were also shown by the mean concentration contours in Fig. 7a–f.

Fig. 8 compares full LES and rCFD for mean K_C along the five vertical lines downstream of the building. In general, the results by full LES and rCFD agree well. rCFD provides some overestimations compared to full LES for heights above roof height, while some underestimations are present at lower heights. Most probably, these remaining discrepancies can be linked to the representation of the exhaust vent by an attached source volume (with a finite height above the top of the building) instead of a non-penetrating velocity inlet face condition. In the current implementation of rCFD, this volumetric representation can be regarded as an intrinsic model requirement, since convection is only addressed by cell-to-cell shifts while face-to-cell shifts are not considered. While this restriction might be alleviated in future versions of rCFD, these discrepancies are accepted at this point, since the magnitude of the deviation is small and the shape of the profiles is recovered to a sufficient degree.

To quantify the agreement between the full LES and the rCFD results, four evaluation metrics are considered here: the fraction of predictions within a factor of two of observations (FAC2), the fractional bias (FB), the normalized mean square error (NMSE) and the linear correlation coefficient (R). FAC2 can be seen as a robust measurement metric and it can represent an overall performance of the rCFD prediction ability [43]. FB is a dimensionless metric, and thus it is convenient for assessing different concentration levels [43]. NMSE can reflect both the systematic and random errors, but both FB and NMSE can be influenced by extreme outliners. R can reflect the linear relationship between full LES and rCFD, and a good R value is necessary for rCFD prediction accuracy [48]. The perfect agreement between full LES and rCFD or the ideal

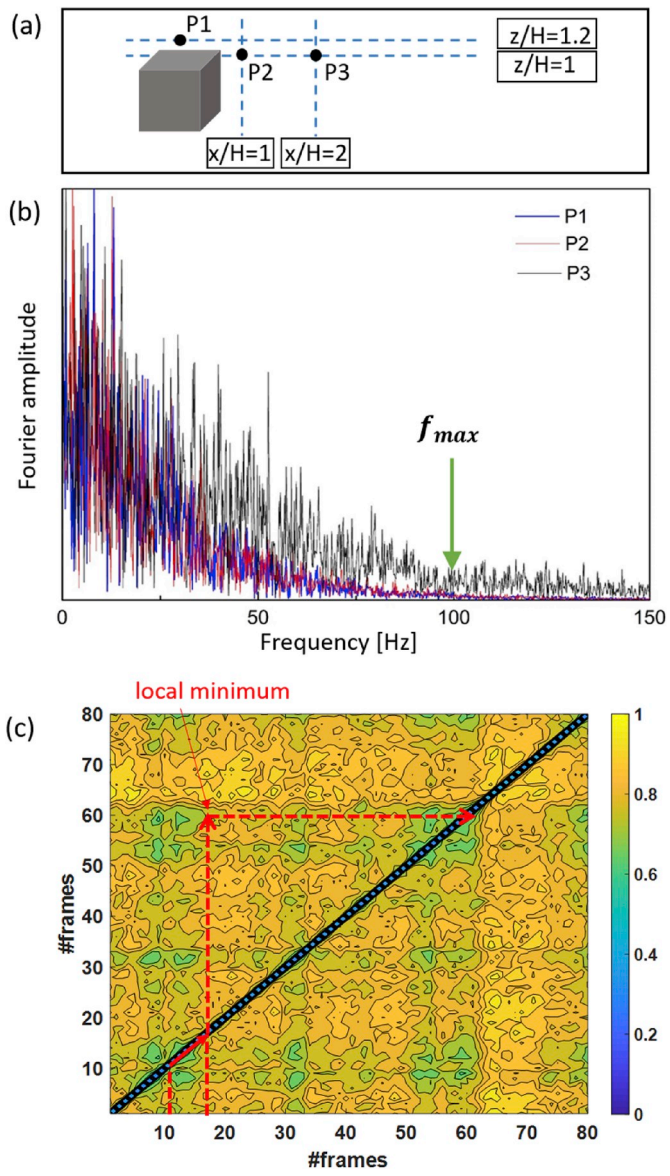

Fig. 6. (a) Position of monitoring points; (b) Spectral analysis of sampling signals; and (c) Plot of rMatrix for 80 frames.

values of FAC2 and R are both 1 and the ideal values of FB and NMSE are both 0. Based on the recommendations from the literature [18,43,49], the suggested good evaluation metrics for K_c are: FAC2 > 0.5, |FB| < 0.3, NMSE <4, and $R > 0.8$. The equations for calculating these metrics are:

$$FAC2 = \frac{1}{n}\sum_i F_i \qquad F_i = \begin{cases} 1, if \;\; 0.5 \le \dfrac{P_r}{P_{LES}} \le 2 \\ 0, else \end{cases} \tag{14}$$

$$FB = \frac{\sum_i (P_r - P_{LES})}{0.5\sum_i (P_r + P_{LES})} \tag{15}$$

$$NMSE = \frac{1}{n}\sum_i (P_r - P_{LES})^2 / (P_r P_{LES}) \tag{16}$$

$$R = \frac{\frac{1}{n}\sum_i (P_r - \langle P_r \rangle)(P_{LES} - \langle P_{LES} \rangle)}{\sigma_{P,r}\sigma_{P_{LES}}} \tag{17}$$

here, P_r and P_{LES} are the predicted results from rCFD and full LES, respectively. $i = 1, \ldots, n$, which are grid points in CFD simulation. Note that full LES and rCFD employ the same grid. The symbol $\langle \cdot \rangle$ indicates averaged value. $\sigma_{P,r}$ and $\sigma_{P,LES}$ are the standard deviations of P_r and P_{LES}, respectively.

The metrics are applied for five vertical lines (see Fig. 8) in accordance with the concentration measurements of Li and Meroney [28,41]. It should be mentioned that the cell nodes in the simulation are used as the evaluation points, and over 60 nodes are involved for each line here. The evaluation results are listed in Table 1. Even though the FAC2 values for the lines farther away from the cubical building are slightly worse than that of the lines closer to building, all the values for FAC2 metric are above 0.87, which is also the case for the average value. This suggests a good agreement between rCFD and full LES results. Most of the FB values are below zero, which means rCFD predicts lower pollutant concentrations than full LES. The values of NMSE are below 0.1, which indicates that the systematic and random errors are both very low. The values of R are over 0.93, suggesting a rather strong linear relationship between rCFD and full LES results. From the above systematic evaluation, it is safe to say that the rCFD simulation can predict very similar results as full LES.

4.3. Results of instantaneous concentration coefficient

The animation of the full LES and rCFD results for the isosurface of concentration coefficient $K_C = 1$for a time period of $t^* = 14$ is presented in Appendix A.

4.4. Results of concentration fluctuation

The comparison of I_c values between full LES and rCFD along the five vertical lines are shown in Fig. 9. It shows that the rCFD results agree well with full LES below building height ($z/H < 1$) for all five lines. The I_c results by rCFD are generally smaller than the full CFD results and the deviation between rCFD and full CFD is relatively large for heights close to 1.5 times of building height. This might be attributed to the limited size of the database. Even if the pseudo-periodic nature of the flow can be captured by the recurrence matrix (i.e. the matrix has a horizontal plateau), the results still miss irregularly occurring rare events of the flow (i.e. low-speed spikes penetrating into the undisturbed flow). It will be very difficult or even impossible to include these rare flow features in the concept of recurrence CFD with its limited databases. Such rare events can be observed in the experiments and captured by full LES but not by rCFD, and thus rCFD underestimates the corresponding I_c values.

The assessment of the agreement between the full LES and rCFD results of I_c by the evaluation metrics is given in Table 2. Similar to the evaluation procedure mentioned above, the cell nodes are used for the evaluation points and more than 50 points are involved here since only 1.5 times the height of the building height is considered. The FAC2 values are mainly influenced by the values near the region of 1.5 times of the cubical building height, but they are still over 0.86 for all lines. All FB values are negative, which suggests an underestimation by rCFD compared to full LES. The absolute values of all the FB metrics are below 0.2. The values of NMSE are close to 0, which is also the case for the average value, which means that the deviations between rCFD and full LES simulation results are small. The R values are all over 0.87, indicting strong linear relationship between the rCFD and full LES simulation results.

4.5. Alternative pollution events

An additional major advantage of rCFD is that different dispersion events can be solved promptly once the database has been stored for the wind flow with the same characteristics, as explained in Section 2. In this subsection, two additional cases with different source locations, e.g. a lateral and a leeward source location, are presented to test the rCFD simulation performance in this aspect. The pollutants (a mixture of helium with air, same as before) are released from the centre of the

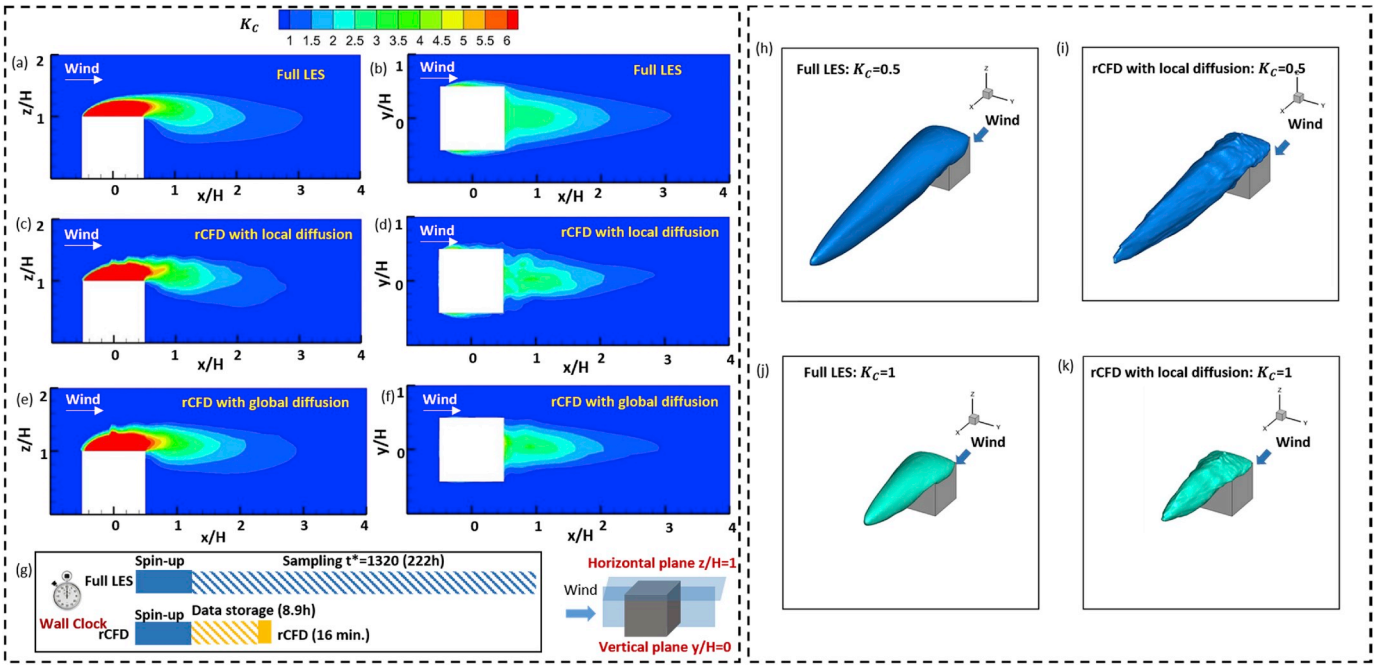

Fig. 7. Comparison of mean concentration coefficient between full LES and rCFD in two planes (a)–(f), and (g) wall-clock time consumption; (h–k) iso-surfaces of time-averaged (t^*=1320) concentration coefficient.

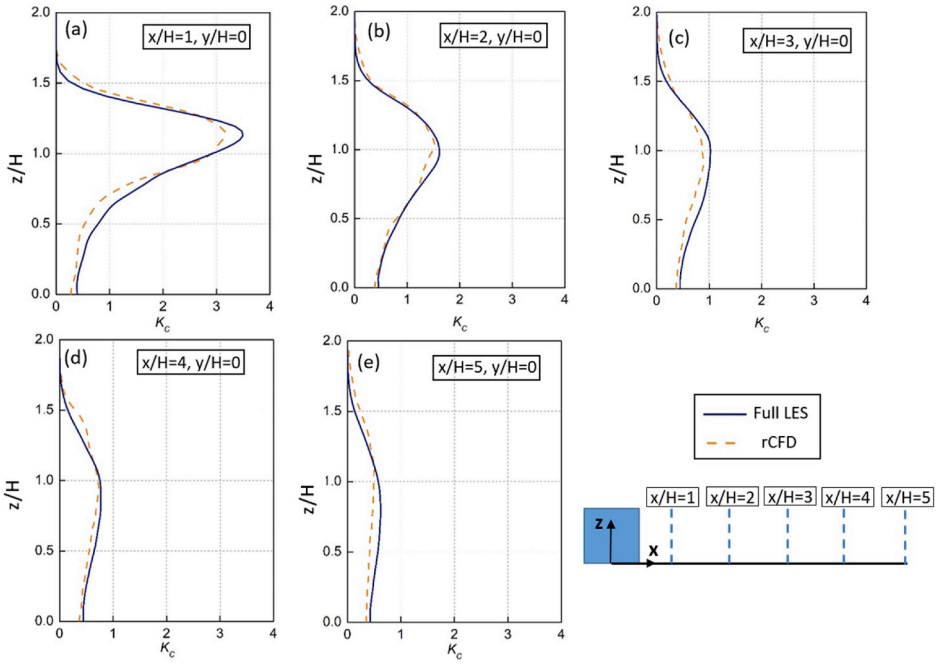

Fig. 8. Comparison of K_C between full LES and rCFD along five vertical lines in the vertical centre-plane downstream of the building.

Table 1
Evaluation metrics for K_C values.

Lines	FAC2	FB	NMSE	R
x/H = 1	0.944	−0.079	0.069	0.988
x/H = 2	0.924	−0.014	0.012	0.994
x/H = 3	0.901	−0.088	0.038	0.989
x/H = 4	0.891	0.055	0.086	0.965
x/H = 5	0.874	−0.017	0.081	0.938
Average value	0.907	−0.029	0.057	0.975

leeward and lateral face of the cubical building, while the release rates and other boundary conditions are the same as in the previous case. The database from Section 4.1 together with the same rCFD parameters are used here for the rCFD simulation.

Fig. 10 presents K_c obtained from full LES and rCFD simulation in two planes when the pollutant source is located in the centre of the leeward face of the cubical building. As shown in Fig. 10e, the wall clock time for the rCFD is only 16 min while the full LES needs 237 h for this case including the spin-up time. Thus, the time consumption is reduced nearly three orders of magnitude (237 h vs 16 min). For both the vertical and horizontal planes, the width and the length of the time-averaged

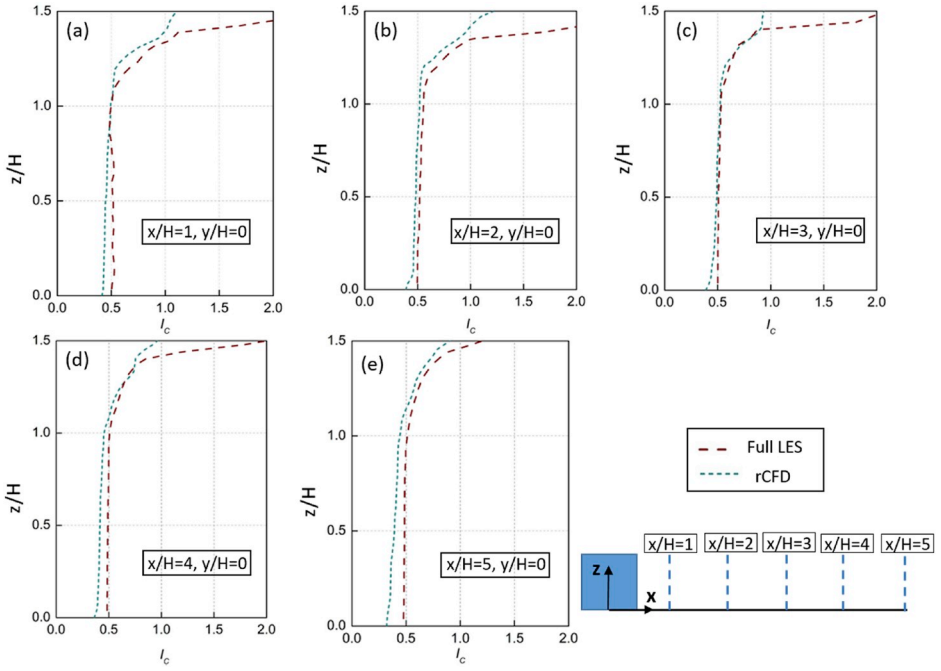

Fig. 9. Comparison of I_c along five vertical lines in the vertical central plane downstream of the building.

Table 2
Evaluation metrics for I_C values.

Lines	FAC2	FB	NMSE	R
x/H = 1	0.865	−0.077	0.012	0.937
x/H = 2	0.878	−0.060	0.011	0.897
x/H = 3	0.903	−0.079	0.033	0.870
x/H = 4	0.901	−0.149	0.036	0.899
x/H = 5	0.952	−0.191	0.044	0.953
Average value	0.901	−0.111	0.027	0.911

concentration plume around the cubical building are very similar between full LES and rCFD (Fig. 10a–d). In addition, the shape and the volume of the time-averaged concentration plumes of $K_C = 1$ are also similar (Fig. 10g,f). As expected, the concentration plumes by rCFD are less smooth compared to those by full LES because of the limited stored database. Note that the full LES plume (Fig. 10f) partly covers the side façade of the cubical building while this is not the case in rCFD (Fig. 10g).

Fig. 11 presents K_c by full LES and rCFD when the pollutant is emitted from the centre of the lateral face of the cubical building. In order to better highlight the differences, a different colorbar is used

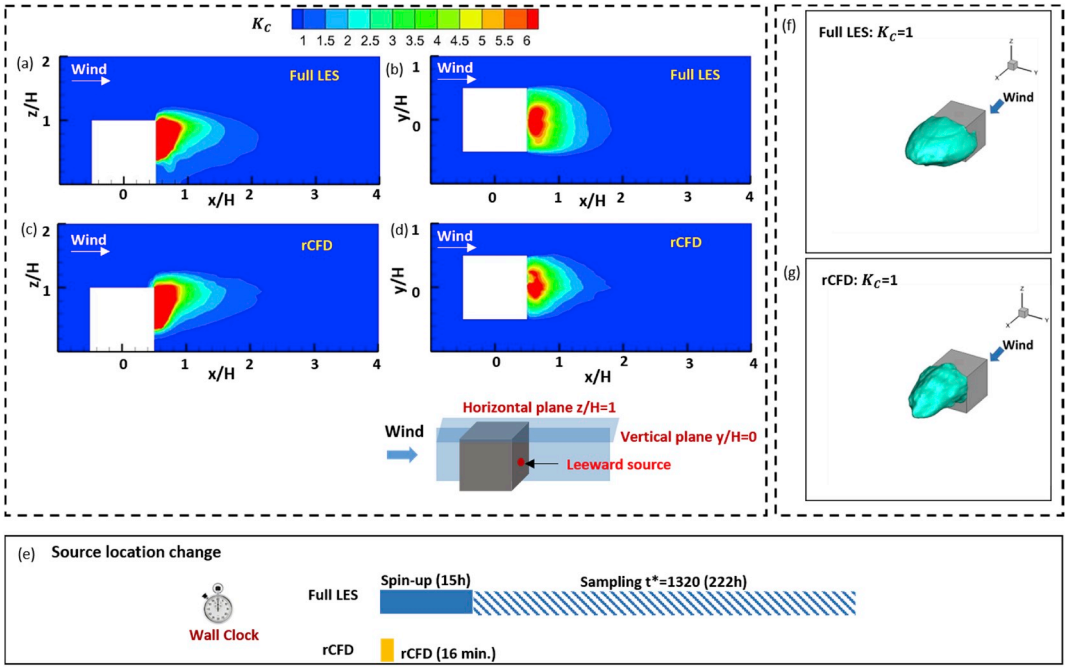

Fig. 10. Comparison of mean concentration coefficient between full LES and rCFD in two planes for the leeward source (a)–(d), and (e) wall-clock time consumption; (f–g) iso-surfaces of time-averaged (t^*=1320) concentration coefficient.

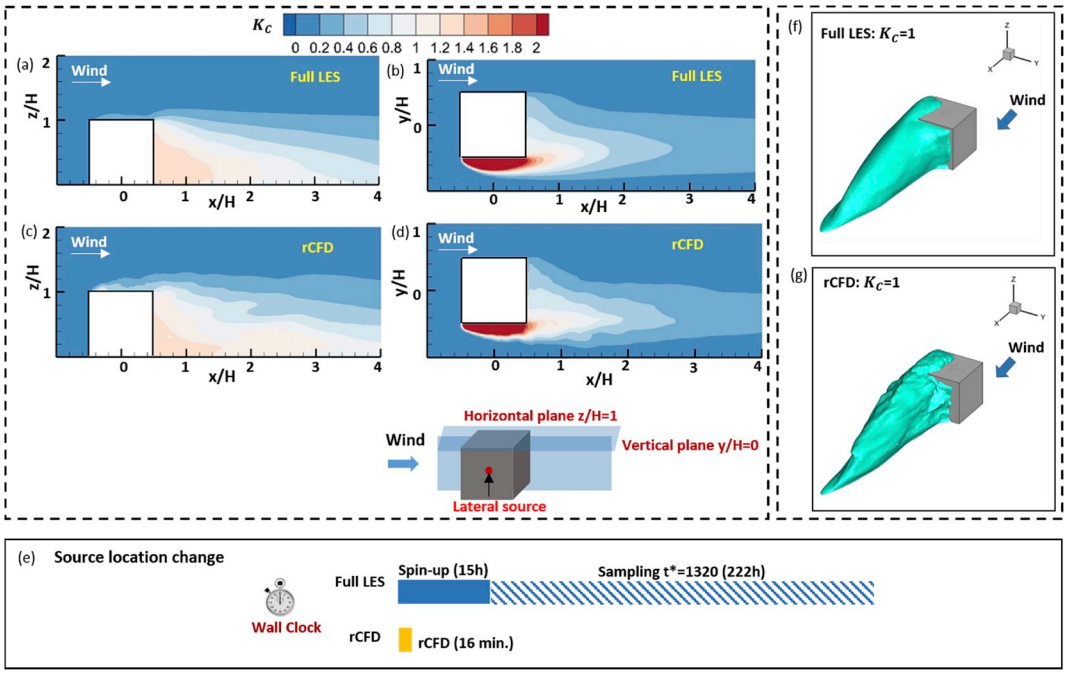

Fig. 11. Comparison of mean concentration coefficient between full LES and rCFD in two planes for the lateral source (a)–(d), and (e) wall-clock time consumption; (f–g) iso-surfaces of time-averaged (t^*=1320) concentration coefficient.

here. In general, the concentration plumes by rCFD are very similar to those by full LES in terms of plume shape and length in downstream of the cubical building. However, the computational time is reduced nearly three orders. Concerning the time-averaged plume shapes of $K_C = 1$ (Fig. 11f vs. g), there are subtle differences between full LES and rCFD.

5. Discussion

In the following subsections, the existing limitations and future challenges of transport-based rCFD as well as aspects of computational performance are discussed.

5.1. Limitations

For the rCFD approach, a sufficient degree of recurrence in the flow under consideration is the strongest requirement/limitation. In typical atmospheric near-field situations, this requirement is certainly fulfilled. Such flows exhibit reappearing flow features (e.g. vortex shedding in the wakes of buildings and separation bubble formation and collapse) which render them pseudo-periodic in the time-scale of passive pollutant dispersion. However, for example in the case of erupting fire plumes, the flow cannot be considered as being pseudo-periodic. Hence, rCFD cannot be applied for flows which have no recurrent flow features.

If the flow under consideration is pseudo-periodic, the recurrent flow features can be stored into a database. Naturally, this database should be limited in size in order to avoid excess storage consumption and to limit the run-time of the underlying full CFD simulation. However, if the database is too small, it will be an insufficient representation of the underlying flow. In Fig. 12, the concentration pattern for the cubical building with central rooftop vent is plotted for a reduced database of only 30 frames. Because of an insufficient database, an artificial asymmetry in the mean concentration plume can be found as shown in Fig. 12. It should be mentioned that the database built in this study is sufficiently large to represent the pseudo-periodic nature of the flow under consideration, even though it does not contain all the information of a full LES simulation. An in-depth discussion on the requirements of

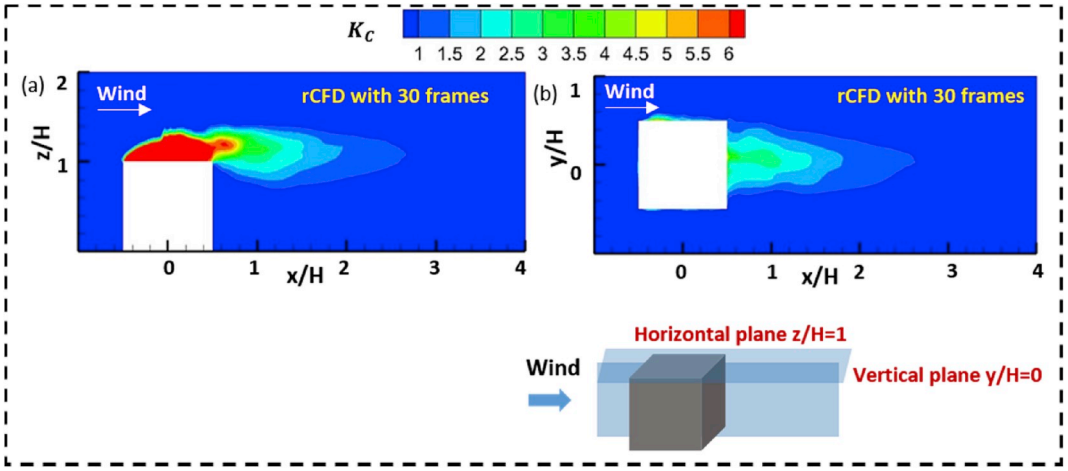

Fig. 12. Mean concentration coefficient for rCFD simulation with 30 frames: (a) vertical centre-plane y/H = 0; and (b) horizontal plane z/H = 0.05.

the database can be found in Ref. [27].

In the present paper, we focused on stationary (i.e. statistically steady conditions), where the time-averaged approach-flow mean wind speed and turbulence intensity are constant and independent of the choice of the averaging interval. This implies that time averaging can be applied, rather than ensemble averaging. However, in reality the approaching wind flow will exhibit instationarity (i.e. a not statistically steady flow) when considering sufficiently long time scales (in previous publications on rCFD such flows were labelled as "recurrent-transient" [37]). Therefore, dedicated databases for every type of wind field under consideration should be established. Naturally, such situations raise the need for an interpolation procedure between databases. While Eulerian velocity fields or Lagrangian cell-to-cell paths cannot be interpolated directly due to the non-linearity of convection, the probability of occurrences of sequences from different databases (i.e. in the sense of sequence-width-modulation) has been successfully interpolated in previous studies [37]. However, the applicability of this approach for atmospheric pollutant dispersion simulation still needs to be proven in further works.

5.2. Performance

Without considering the time needed for establishing the database (which has to be built only once for stationary flows), the presented version of rCFD results in a computational speed-up close to three orders of magnitude compared to corresponding full LES simulations (i.e. 16 min versus 222 h). However, in previous applications of rCFD in the field of chemical engineering [27,37], the rCFD approach reduces the simulation time by over four orders of magnitude. This can be partly attributed to the novel sophisticated modelling of physical (data-driven) diffusion (Section 2.3). In fact, the computational time for rCFD can be reduced to 20 s in case a rough one-step diffusion for mass/species conservation is used [27]. The improvement of the computational performance for the pollutant dispersion application will be explored in further work.

6. Conclusion

In this paper, the novel transport-based rCFD is applied for the first time to simulate atmospheric pollutant dispersion in the built environment. Another novelty of the transport-based rCFD applied in this paper is that the diffusion factor is related to the local sub-grid diffusivity (novel diffusion model), which enhances the modelling accuracy of pollutant dispersion. The applicability of rCFD is evaluated for the case of pollutant dispersion around an isolated cubical building in a neutral atmospheric boundary layer. The results by full LES are first validated based on previously published wind tunnel data and then used to evaluate the accurate of rCFD. The main findings are concluded as follows:

(i) For the time-averaged pollutant concentration, the results by full LES and rCFD are very close to each other, as shown by (a)concentration coefficients along five lines; (b)concentration coefficient contours in a horizontal and a vertical plane; and (c) 3D plume shapes based on isosurfaces of mean concentration coefficient.
(ii) The rCFD simulation can predict similar pollutant concentration fluctuations as full LES, except for the regions above the upper bound of the free shear layer, which is attributed to the limited database used in the current study.
(iii) Using rCFD instead of full LES, the computational time is reduced by nearly three orders of magnitude (16 min vs. 222 h).
(iv) rCFD with the novel diffusion model shows substantially improved quantitative accuracy compared to the method with the global diffusion factor. This improvement can be attributed to the fact that the novel diffusion model is directly related to the local subgrid diffusivity.
(v) FAC2, FB, NMSE, and R between rCFD and full LES for the mean concentration coefficient are calculated along five vertical lines in the vertical central plane downstream of the building. The average values of these evaluation metrics are 0.907, −0.029, 0.057 and 0.975, respectively, indicating a very good agreement between rCFD and full LES.
(vi) FAC2, FB, NMSE, and R for local pollutant fluctuation intensity along the same five vertical lines have averaged values of 0.901, −0.111, 0.027 and 0.911, respectively, also indicating a good agreement between rCFD and full LES.

In addition, rCFD has the favourable feature that different pollutant dispersion cases can be solved promptly once the database has been established for a given flow under consideration. This advantage has been demonstrated by changing the pollutant source (vent) position first to the leeward face and then to the lateral face of the cubical building. Also in these cases, rCFD agreed very well with full LES.

In conclusion, this paper demonstrates the applicability and the potential of transport-based rCFD in the field of atmospheric pollutant dispersion in the built environment.

Declaration of competing interest

The authors declare that they have no known competing financial interests or personal relationships that could have appeared to influence the work reported in this paper.

Acknowledgement

The authors acknowledge the financial contribution of the Linz Institute of Technology (LIT-2017-3-SEE-008).

Appendix B. Supplementary data

Supplementary data to this article can be found online at https://doi.org/10.1016/j.buildenv.2019.106604.

Appendix A. Instantaneous concentration plume (animation)

Animation file: Instantaneous concentration plume from full LES and rCFD: isosurface $K_C = 1$ (nontransparent) and iso-surface $K_C = 0.5$ (transparent).

References

[1] M. Lateb, R.N. Meroney, M. Yataghene, H. Fellouah, F. Saleh, M.C. Boufadel, On the use of numerical modelling for near-field pollutant dispersion in urban environments–A review, Environ. Pollut 208 (2016) 271–283.

[2] P. Gousseau, B. Blocken, T. Stathopoulos, G.J.F. van Heijst, CFD simulation of near-field pollutant dispersion on a high-resolution grid: a case study by LES and RANS for a building group in downtown Montreal, Atmos, Environ. Times 45 (2011) 428–438.

[3] J. Hang, Y. Li, M. Sandberg, R. Buccolieri, S. Di Sabatino, The influence of building height variability on pollutant dispersion and pedestrian ventilation in idealized high-rise urban areas, Build. Environ. 56 (2012) 346–360.

[4] Z. Ai, C.M. Mak, From street canyon microclimate to indoor environmental quality in naturally ventilated urban buildings: issues and possibilities for improvement, Build. Environ. 94 (2015) 489–503.

[5] ASHRAE, ASHRAE Handbook: Fundamentals, American Society of Heating Refrigerating and Air-Conditioning Engineers, Atlanta, 2005.

[6] S.R. Hanna, B.A. Egan, J. Purdum, J. Wagler, Evaluation of the ADMS, AERMOD, and ISC 3 dispersion models with the OPTEX, duke forest, kincaid, indianapolis and lovett field datasets, Int. J. Environ. Pollut. 16 (2001) 301–314.

[7] A.C. Stern, Air Pollution: Air Pollutants, Their Transformation and Transport, Academic Press, New York, USA, 1976.

[8] B. Hajra, T. Stathopoulos, A. Bahloul, Assessment of pollutant dispersion from rooftop stacks: ASHRAE, ADMS and wind tunnel simulation, Build. Environ. 45 (2010) 2768–2777.

[9] B. Hajra, T. Stathopoulos, A. Bahloul, The effect of upstream buildings on near-field pollutant dispersion in the built environment, Atmos. Environ. 45 (2011) 4930–4940.

[10] Y. Tominaga, T. Stathopoulos, CFD simulation of near-field pollutant dispersion in the urban environment: a review of current modeling techniques, Atmos. Environ. 79 (2013) 716–730.

[11] B. Blocken, T. Stathopoulos, J. Carmeliet, J.L. Hensen, Application of computational fluid dynamics in building performance simulation for the outdoor environment: an overview, J. Build. Perform. Simu. 4 (2011) 157–184.

[12] J. Hang, Z. Luo, X. Wang, L. He, B. Wang, W. Zhu, The influence of street layouts and viaduct settings on daily carbon monoxide exposure and intake fraction in idealized urban canyons, Environ. Pollut. 220 (2017) 72–86.

[13] L. Chen, J. Hang, M. Sandberg, L. Claesson, S. Di Sabatino, H. Wigo, The impacts of building height variations and building packing densities on flow adjustment and city breathability in idealized urban models, Build. Environ. 118 (2017) 344–361.

[14] Y. Du, C.M. Mak, Z. Ai, Modelling of pedestrian level wind environment on a high-quality mesh: a case study for the HKPolyU campus, Environ. Model. Softw. 103 (2018) 105–119.

[15] Y. Du, C.M. Mak, J. Liu, Q. Xia, J. Niu, K.C. Kwok, Effects of lift-up design on pedestrian level wind comfort in different building configurations under three wind directions, Build, Environ. Times 117 (2017) 84–99.

[16] Y. Tominaga, T. Stathopoulos, Numerical simulation of dispersion around an isolated cubic building: comparison of various types of k–ϵ models, Atmos. Environ. 43 (2009) 3200–3210.

[17] B. Blocken, Computational Fluid Dynamics for urban physics: importance, scales, possibilities, limitations and ten tips and tricks towards accurate and reliable simulations, Build. Environ. 91 (2015) 219–245.

[18] Y. Tominaga, T. Stathopoulos, CFD simulations of near-field pollutant dispersion with different plume buoyancies, Build. Environ. 131 (2018) 128–139.

[19] B. Blocken, LES over RANS in building simulation for outdoor and indoor applications: a foregone conclusion? Building Simulation Build. Simul. 11 (2018) 821–870.

[20] P. Gousseau, B. Blocken, G.J.F. van Heijst, Large-Eddy Simulation of pollutant dispersion around a cubical building: analysis of the turbulent mass transport mechanism by unsteady concentration and velocity statistics, Environ. Pollut. 167 (2012) 47–57.

[21] D. Hertwig, G. Patnaik, B. Leitl, LES validation of urban flow, part I: flow statistics and frequency distributions, Environ. Fluid Mech. 17 (2017) 521–550.

[22] P. Moonen, C. Gromke, V. Dorer, Performance assessment of Large Eddy Simulation (LES) for modeling dispersion in an urban street canyon with tree planting, Atmos. Environ. 75 (2013) 66–76.

[23] S.M. Salim, R. Buccolieri, A. Chan, S. Di Sabatino, Numerical simulation of atmospheric pollutant dispersion in an urban street canyon: comparison between RANS and LES, J. Wind Eng. Ind. Aerodyn. 99 (2011) 103–113.

[24] Y. Tominaga, T. Stathopoulos, CFD modeling of pollution dispersion in building array: evaluation of turbulent scalar flux modeling in RANS model using LES results, J. Wind Eng. Ind. Aerodyn. 104 (2012) 484–491.

[25] Z.T. Ai, C.M. Mak, Large eddy simulation of wind-induced interunit dispersion around multistory buildings, Indoor Air 26 (2016) 259–273.

[26] P. Moonen, V. Dorer, J. Carmeliet, Effect of flow unsteadiness on the mean wind flow pattern in an idealized urban environment, J. Wind Eng. Ind. Aerodyn. 104 (2012) 389–396.

[27] S. Pirker, T. Lichtenegger, Efficient time-extrapolation of single- and multiphase simulations by transport based recurrence CFD (rCFD), Chem. Eng. Sci. 188 (2018) 65–83.

[28] W.-W. Li, R.N. Meroney, Gas dispersion near a cubical model building. Part I. Mean concentration measurements, J. Wind Eng. Ind. Aerodyn. 12 (1983) 15–33.

[29] P. Gousseau, B. Blocken, G.J.F. van Heijst, CFD simulation of pollutant dispersion around isolated buildings: on the role of convective and turbulent mass fluxes in the prediction accuracy, J. Hazard Mater. 194 (2011) 422–434.

[30] Y. Tominaga, T. Stathopoulos, Numerical simulation of dispersion around an isolated cubic building: model evaluation of RANS and LES, Build. Environ. 45 (2010) 2231–2239.

[31] F. Bazdidi-Tehrani, A. Ghafouri, M. Jadidi, Grid resolution assessment in large eddy simulation of dispersion around an isolated cubic building, J. Wind Eng. Ind. Aerodyn. 121 (2013) 1–15.

[32] F. Bazdidi-Tehrani, A. Mohammadi-Ahmar, M. Kiamansouri, M. Jadidi, Investigation of various non-linear eddy viscosity turbulence models for simulating flow and pollutant dispersion on and around a cubical model building, Build. Simul. 8 (2015) 149–166.

[33] G. Berkooz, P. Holmes, J.L. Lumley, The proper orthogonal decomposition in the analysis of turbulent flows, Annu. Rev. Fluid Mech. 25 (1993) 539–575.

[34] K. Taira, S.L. Brunton, S.T. Dawson, C.W. Rowley, T. Colonius, B.J. McKeon, O. T. Schmidt, S. Gordeyev, V. Theofilis, L.S. Ukeiley, Modal analysis of fluid flows: an overview, AIAA J. (2017) 4013–4041.

[35] T. Lichtenegger, E.A.J.F. Peters, J.A.M. Kuipers, S. Pirker, A recurrence CFD study of heat transfer in a fluidized bed, Chem. Eng. Sci. 172 (2017) 310–322.

[36] T. Lichtenegger, S. Pirker, Recurrence CFD–a novel approach to simulate multiphase flows with strongly separated time scales, Chem. Eng. Sci. 153 (2016) 394–410.

[37] S. Pirker, T. Lichtenegger, Process control of through-flow reactor operation by real-time recurrence CFD (rCFD) simulations – proof of concept, Chem. Eng. Sci. 198 (2019) 241–252.

[38] ANSYS Fluent 19.0. Theory Guide, ANSYS Inc., 2018.

[39] J. Smagorinsky, General circulation experiments with the primitive equations: I. The basic experiment, Mon. Weather Rev. 91 (1963) 99–164.

[40] C. Kloss, C. Goniva, A. Hager, S. Amberger, S. Pirker, Models, algorithms and validation for opensource DEM and CFD–DEM, progress in computational fluid dynamics, an International Journal Prog. Comput. Fluid Dy. 12 (2012) 140–152. http://www.liggghts.com.

[41] W.-W. Li, R.N. Meroney, Gas dispersion near a cubical model building. Part II. Concentration fluctuation measurements, J. Wind Eng. Ind. Aerodyn. 12 (1983) 35–47.

[42] Y. Tominaga, A. Mochida, R. Yoshie, H. Kataoka, T. Nozu, M. Yoshikawa, T. Shirasawa, AIJ guidelines for practical applications of CFD to pedestrian wind environment around buildings, J. Wind Eng. Ind. Aerodyn. 96 (2008) 1749–1761.

[43] M. Schatzmann, H. Olesen, J. Franke, COST 732 Model Evaluation Case Studies: Approach and Results, COST Office, Brussels, Belgium, 2010.

[44] J. Franke, Best Practice Guideline for the CFD Simulation of Flows in the Urban Environment, Meteorological Inst, 2007.

[45] T.V. Hooff, B. Blocken, Coupled urban wind flow and indoor natural ventilation modelling on a high-resolution grid: a case study for the Amsterdam ArenA stadium, Environ. Model. Softw 25 (2010) 51–65.

[46] P.G. Tucker, A. Mosquera NAFEMS introduction to grid and mesh generation for CFD NAFEMS CFD, Working Group (2001) 56. R0079.

[47] F. Mathey, D. Cokljat, J.-P. Bertoglio, E. Sergent, Specification of LES inlet boundary condition using vortex method, in: Fourth International Symposium on Turbulence, Heat and MassTransfer, 2006. Antalya, Turkey.

[48] J.C. Chang, S.R. Hanna, Air quality model performance evaluation, Meteorol. Atmos. Phys. 87 (2004) 167–196.

[49] S.R. Hanna, O.R. Hansen, S. Dharmavaram, FLACS CFD air quality model performance evaluation with Kit Fox, MUST, Prairie Grass, and EMU observations, Atmos. Environ. 38 (2004) 4675–4687.